Title: Reactive oxygen species trigger downward vertical migration in diatom microphytobenthic biofilms as a strategy to cope with oxidative stress

Short title: ROS-Triggered Diatom Biofilm Migration

Authors' information:

1. Alexandre Desparmet[1] (alexandre.desparmet@mnhn.fr ; ORCID 0009-0009-6783-277X)
2. Bruno Jesus[2] (bruno.jesus@univ-nantes.fr ; ORCID 0000-0002-2047-3783)
3. Tony Robinet[1] (tony.robinet@mnhn.fr ; ORCID 0000-0002-3669-2788)
4. Thierry Dufour[3] (thierry.dufour@sorbonne-universite.fr ; ORCID 0000-0002-0397-368X)
5. Cédric Hubas[1] (cedric.hubas@mnhn.fr ; ORCID 0000-0002-9110-9292)

[1]Laboratoire de Biologie des Organismes et Écosystèmes Aquatiques (BOREA), UMR 8067, Muséum National d'Histoire Naturelle, Sorbonne Université, CNRS 7208, IRD 207, UCN, UA, Station Marine de Concarneau, Quai de la Croix, 29900 Concarneau, France.

[2]Institut Des Substances et Organismes de la Mer (ISOMer), UR 2160, Nantes université, Faculté des Sciences et des Techniques, 44000 Nantes, France.

[3]Laboratoire de Physique des plasmas (LPP), UMR 7648, Sorbonne Université, CNRS, École Polytechnique, Univ. Paris-Sud, Observatoire de Paris, Université Paris-Saclay, PSL Research University, 4 Place Jussieu, 75252 Paris, France.

Corresponding author:

Alexandre Desparmet
Laboratoire de Biologie des Organismes et Écosystèmes Aquatiques (BOREA), UMR 8067, Muséum National d'Histoire Naturelle, Sorbonne Université, CNRS 7208, IRD 207, UCN, UA, Station Marine de Concarneau, Quai de la Croix, 29900 Concarneau, France.
alexandre.desparmet@mnhn.fr ; ORCID 0009-0009-6783-277X

ABSTRACT

Diatom-dominated intertidal microphytobenthic biofilms experience daily fluctuations in irradiance, which can lead to oxidative stress within the photosynthetic apparatus through the production and accumulation of reactive oxygen species. To maintain photosynthetic efficiency, benthic diatoms have developed protective strategies, including mobilization of the antioxidant xanthophyll cycle and the ability to migrate vertically through sediments. However, mechanistic understanding of signaling pathways underlying migration remains poorly characterized. This study investigated the triggering effect of reactive oxygen species on behavioral and photophysiological responses through the analysis of lipophilic pigments and fluorescence parameters. To this end, two microphytobenthic communities, one with sediment allowing vertical migration and another without sediment restricting it, were exposed to irradiance, cold atmospheric plasma, and hydrogen peroxide stresses. Results showed a consistent downward migration response under all oxidative stresses, highlighting the key role of reactive oxygen species, especially hydrogen peroxide, in triggering this microphytobenthic behavior. Moreover, a difference was observed between the pathways involved in vertical migration and those underlying photoprotective responses. Hydrogen peroxide and cold atmospheric plasma stresses highlighted the necessity for substantial microphytobenthic migration, whereas irradiance induced a specific and controlled response involving engagement of the xanthophyll cycle, acting in synergy with the migration strategy by showing stronger activation when migration was impaired. By establishing that a rapid and efficient migration could be induced by reactive oxygen species and could act in synergy with the xanthophyll cycle in epipelic cells, this study provides key insights into the molecular basis of microphytobenthic responses to cellular and environmental oxidative stresses.

Key Words: *Diatom microphytobenthic biofilms | Pleurosigma strigosum | Vertical migration | ROS | Light stress | Cold Atmospheric Plasma | Hydrogen peroxide | Xanthophyll cycle | Photophysiology*

Abbreviations: *Minimum dark-adapted fluorescence yield,* F_0*; Maximum quantum yield of photosystem II photochemistry under dark-adapted state, Fv/Fm; Non-photochemical quenching, NPQ; Relative electrons transport rate, rETR; Reactive oxygen species, ROS; Non-regulated non-photochemical quenching energy dissipation, Y(NO); Regulated non-photochemical quenching, Y(NPQ).*

INTRODUCTION

The aquatic microbiome exhibits a remarkable diversity of adaptive strategies to deal with rapid environmental fluctuations. Intertidal sediments, as dynamic interfaces, undergo significant qualitative and quantitative variations in the electromagnetic spectrum throughout

the day, impacting the phototrophic communities[1]. Among these, microphytobenthos dominated by epipelic diatoms, forms structured mucilaginous biofilms on muddy substrata, an advantageous lifestyle that plays a key role in their adaptation and associated ecosystem services[2–4].

Light carries essential environmental information that diatoms can perceive either directly through photoreceptors or indirectly via cellular signals, such as levels of reactive oxygen species (ROS) and the redox state of the photosynthetic chain[5–7]. These signals trigger physiological responses involved in light acclimation, photoprotection and photomotile movements, enabling diatoms to acclimate, adapt, and survive[8]. Under high light intensity conditions, photosynthetic capacity can be exceeded, leading to the synthesis and accumulation of ROS, natural by-products of oxygen metabolism, including singlet oxygen $^1O_2$, superoxide $O_2^{\bullet -}$, hydrogen peroxide H_2O_2 (e.g. via the Mehler reaction), and hydroxyl $HO^\bullet$[9]. This deregulation disrupts homeostasis and causes photooxidative damage, such as lipid peroxidation, which compromises cellular integrity[10], and the oxidation of DNA and key proteins such as the photosystem II D1 protein[11, 12], which can ultimately result in cell death[9, 13]. Epipelic diatoms have developed two major adaptive strategies to preempt this ROS formation and accumulation, ensuring optimal photosynthetic processes in a variable light environment: vertical migration behavior and xanthophyll cycle[14, 15].

First described in 1907 by Fauvel and Bohn, the ability of cells to move vertically through muddy substrata is a behavior regulated both endogenously and plastically by various environmental forcing, including light information[16–21]. Rapid and temporally adjustable, this actin-myosin-driven gliding system involving the secretion of extracellular mucilage fibrils through the slit raphe, enables diatoms to quickly reposition themselves at low metabolic cost, allowing them to reach sediment layers with optimal irradiance conditions[20–26]. This adaptation, partly responsible for the diversity of Bacillariophyta[27], represents a significant evolutionary advantage and has given rise to distinct migration strategies depending on species, previous light photoacclimation, and the environmental context[15, 17, 19, 20]. In addition, the optimization of diatom light harvesting results from the dynamic regulation of accessory carotenoid pigments, such as xanthophylls linked with the photosystem II Fucoxanthin-Chlorophyll-Protein supercore complex[6, 14, 28, 29]. Overstimulation of the photosynthetic electron transport chain acidifies the thylakoid lumen through proton translocation associated with the cytochrome b6f complex via the Q-cycle, as well as proton release generated by water photolysis at photosystem II. Under these low-lumen-pH conditions, the enzymatic activity of Diadinoxanthin de-epoxidase is upregulated, leading to the de-epoxidation of Diadinoxanthin embedded in the thylakoid membranes[15, 29–31]. Rapid xanthophyll adjustments involved in the energy-dependent component of non-photochemical quenching (qE) are particularly pronounced in diatoms. This represents a

118 crucial antioxidant photoprotective response that optimizes thermal dispersion of excess
119 energy in a fluctuating environment, thereby limiting ROS-associated damage in the
120 chloroplast[15, 29–31]. These two major adaptations are complemented by others, such as
121 chloroplast mobility[32, 33], spatial cell orientation[34, 35], frustule nanostructures[36], and
122 cellular ROS management through enzymatic and non-enzymatic antioxidant capacities[31,
123 37–39]. Together, these adaptations form a sophisticated system that enables diatoms to
124 monitor and respond to environmental fluctuations, contributing to their success in modern
125 marine ecosystems[6].

126 Although diatom photoregulation via vertical migration and the xanthophyll cycle are both
127 well characterized individually, the mechanistic understanding of molecular ROS-related
128 cellular signaling pathways that coordinate and integrate real-time protective strategies
129 remains poorly understood in benthic diatoms. The present study, conducted on a natural
130 epipelic microphytobenthic biofilm, addresses this gap by testing the hypothesis that: (1) ROS
131 can act as a trigger signal for downward vertical migration, and (2) ROS-induced migration
132 may be initiated through pathways that operate independently of photoprotection.

133 MATERIALS AND METHODS

134 Biofilm sampling and experimental treatments

135 **Microphytobenthos sampling.** Microphytobenthos was collected from a disused outdoor
136 breeding pond at the Concarneau Marine Station (France; 47°52’05.85”N; 3°55’00.51”W).
137 The pond retains at least 5 cm of seawater above the sediment at low tide, ensuring that the
138 biofilm developing on fine-grained muddy sediments under a semi-diurnal tidal regime
139 remains permanently immersed (Fig. 1A, B). The upper centimeter of sediment was sampled
140 at low tide on 29 April 2024 (1:00 PM) using a shovel. Muddy samples were placed in plastic
141 boxes with overlying seawater and left to settle under natural ambient laboratory light
142 conditions, without direct illumination, for 24 hours at 20°C.
143
144 **Community and replicate conditioning.** Two communities were compared: one capable of
145 vertical migration through sediment, exhibiting a robust and regular pattern driven by both
146 endogenous circadian and tidal rhythms (sediment-associated biofilm), and another in which
147 vertical movement was impaired due to the absence of sediment (sediment-free biofilm).
148 Petri dishes (5.5 cm diameter) containing sediment-associated biofilms were prepared 24
149 hours before the experiment, whereas Petri dishes containing sediment-free biofilms were
150 prepared on the day of the experiment from biofilm that had settled in a box for 24 hours. The
151 sediment-associated biofilms consisted of homogeneous sediment discs (5 mm thick) topped

with 4 mL of filtered seawater from Concarneau Bay, which were left to settle for 24 hours under ambient laboratory light and temperature. The sediment-free biofilms were prepared by gently peeling off the highly cohesive, EPS-rich upper millimeter of the microphytobenthos with tweezers and resuspending it in filtered site seawater (ratio 1 mg : 20 mL). This method minimizes mechanical disturbance and preserves the surface community's cell-size distribution and taxonomic composition. Four milliliters of the sediment-free biofilm suspension were placed in each Petri dish.

Oxidative treatments. Both sediment-associated and sediment-free biofilm communities were exposed in the morning (9:00 AM to 1:00 PM), during the biofilm's upward migration phase, to three short oxidative stress treatments. These were compared with dark-adapted controls (<5 µmol photons m^{-2} s^{-1}, which is not complete darkness, but remains below the light compensation point for microphytobenthos[40]). The high-light stress was applied to mimic intense irradiance commonly experienced by autotrophic cells in natural environments, with a 30-minute exposure to 1500 µmol photons m^{-2} s^{-1} of full-spectrum warm white LED light panel (supplementary Fig. 1A). A cold atmospheric plasma was applied for 10 minutes by piezoelectric discharge, using ambient laboratory air as the carrier gas. Exposure was performed indirectly using plasma-activated seawater, with a 3 mm gap maintained between the water surface and the plasma source to prevent mechanical disturbance of diatoms from transient thermal filaments. This treatment generates both reactive oxygen and nitrogen species (*e.g.* H_2O_2, NO_2^-, and NO_3^-), inducing a composite oxidative stress predominantly driven by H_2O_2, which reaches a concentration of 209 µM (additional plasma details provided in the supplementary materials and methods). Finally, we applied a targeted hydrogen peroxide stress, consisting of a 10-minute exposure to a 200 µM H_2O_2 seawater solution, allowing the specific effect of this ROS to be isolated. The H_2O_2 concentration was determined based on the amount produced during the 10-minute plasma treatment, ensuring that the hydrogen peroxide and plasma stresses were as comparable as possible. Both hydrogen peroxide and plasma exposures were conducted in darkness. For sequencing-based community characterization and pigment analyses, five biological replicates ($n = 5$) per community and treatment, all originating from the same initial sampling, were immediately frozen with liquid nitrogen after exposure, lyophilized, and stored at -80°C. Three additional replicates ($n = 3$) were dedicated to photophysiological parameter measurements (Table 1). Additional details on biofilm sampling and experimental treatments are provided in the supplementary materials and methods.

Table 1. Experimental setup

Summary of the materials and treatments tested in this study.

Treatments	Dark-adapted control	High-light	Cold atmospheric plasma	Hydrogen peroxide
Description	Negative control	Natural behavior control	Experimental composite treatment	Positive control
Stress type	-	Warm white UV to near-IR light	Reactive oxygen and nitrogen species stress	Targeted oxidative stress (H_2O_2)
Time exposure	-	30 min	10 min	10 min
ROS origin	-	Endogenous	Exogenous	Exogenous
Experimental materials	Leave in darkness	LED panel Rhino Series (GR-RHINO 260-PRO-DIM)	Plasma activated seawater (PiezoBrush PZ3 with NearField insert from Reylon Plasma GmbH), leave in darkness	Seawater concentrated with H_2O_2 (ref. 216763 from Sigma Aldrich), leave in darkness
Molecular analyses	Sediment-associated biofilm, *n = 5*; Sediment-free biofilm, *n = 5*			
Photophysiological measurements	Sediment-associated biofilm, *n = 3*; Sediment-free biofilm, *n = 3*			

18S rRNA gene amplicon sequencing

To identify the motile diatoms involved in vertical migration behavior, the eukaryotic microphytobenthic community was characterized through a short-read sequencing on a NovaSeq 6000 System (Illumina). DNA was extracted using the NucleoSpin Soil Mini kit (MACHEREY-NAGEL, ref. 740780.10), and the V4 region of the 18S rRNA gene was amplified using primers TAReuk454FWD1 and TAReukREV3[41]. Library construction and sequencing were performed by the company Biomarker Technologies (BMKGENE) GmbH (Münster, Germany).

Chlorophyll fluorescence: Pulse Amplitude Modulated fluorometry

In order to monitor cellular efficiency under the different treatments and interpret subsequent photoprotective responses, photosynthetic parameters derived from Chlorophyll *a* fluorescence were measured using a MonitoringPen MP 100-E (Photon System Instruments). The light curve program consisted of seven one-minute irradiance steps, increasing from 10 to 1000 µmol photons m^{-2} s^{-1} ($\lambda_{LED\ excitation}$ = 470 nm), with consistent gain, superpulse, and flashpulse intensity settings maintained across all measurements. The initial linear α-slope, representing the maximum light use efficiency of photosystem II, was derived from the light-use-efficiency photosynthesis-irradiance (P-E) curves using a previously described and modified model[42, 43]. The relative electron transport rate (rETR) of photosystem II, an indicator of productivity[23] and in some cases a proxy for carbon

209 fixation[44], corresponds to the values extracted directly from light curve points. The
210 maximum quantum yield of photosystem II photochemistry under dark-adapted state
211 (Fv/Fm), as well as non-photochemical quenching (NPQ) and its regulated Y(NPQ) and non-
212 regulated Y(NO) components, were calculated using established equations[45, 46]
213 (supplementary Table 1). All fluorescence measurements of photosynthetic parameters for
214 each sample and treatment were performed twice: once before and once after stress
215 exposure, each time following a minimum dark adaptation period of 10 minutes. After the
216 high-light exposure, post-stress measurements were taken after this dark adaptation period
217 once the exposure had ended, whereas for the hydrogen peroxide and plasma,
218 measurements were performed immediately after the 10-minute stress period, as the
219 samples were already dark-adapted under these treatments. For the dark-adapted control
220 samples, which do not receive any stress, measurements were performed in parallel with the
221 experimental samples, ensuring that they were in the same temporal framework.

222 Monitoring of vertical migration

223 To assess the vertical migratory response over time, the minimum fluorescence of dark-
224 adapted samples (F_0), used as a proxy of surface algal biomass[14, 17], was monitored in
225 the sediment-associated biofilm community after a 24-hour settling period under ambient
226 laboratory light and temperature. F_0 measurements were conducted independently and
227 randomly on dense biofilms (182 cm²) contained in 14 × 13 cm boxes (one box per stress),
228 then compared with their respective dark-adapted biofilms (high-light and plasma: $n = 8$;
229 hydrogen peroxide: $n = 5$). Due to the rapid induction of the migratory response in
230 microphytobenthos, F_0 biomass monitoring was resumed after 5 minutes of dark adaptation
231 following the end of the high-light stress, and immediately after the hydrogen peroxide and
232 plasma stresses.

233 Lipophilic pigments analysis

234 To characterize the metabolic impact of the treatments and complement the photosynthetic
235 efficiency data, the lipophilic pigments were extracted according to a previously published
236 method[47]. Freeze-dried samples (10 mg of sediment-free biofilm and 40 mg of sediment-
237 associated biofilm) were incubated for 15 minutes at -21°C in 2 mL of 95% methanol buffered
238 with 2% ammonium acetate, then filtered through a 0.2µm PTFE filter. Aliquots of 100 µL
239 were injected into an Agilent 1260 Infinity HPLC system equipped with a C18 Supelcosil
240 column and a UV-VIS photodiode array detector (DAD 1260 VL, 250-900 nm). The method
241 employed a flow rate of 0.6 mL min^{-1} using solvent mixture A (0.5M ammonium acetate in
242 85:15 methanol:water), B (90:10 acetonitrile:water), and C (100% ethyl acetate). A total of 44

243 microphytobenthic pigments were detected (list and abbreviations are provided
244 supplementary Table 2), and their concentrations (µg pigment g^{-1} dry weight) were quantified
245 using calibration curves based on phytoplankton pigment standards from DHI. Two groups of
246 derived Chlorophyll *a* were identified: the "Chlorophyll *a*-derivatives" group includes
247 unidentified Chlorophyll *a*-like pigments, as well as the allomer, and epimer forms; the
248 "Pheopigments" group includes Pheophytins *a*, Pheophorbides *a*, and Pyropheophytin *a*. The
249 contribution (%) of each Chlorophyll *a*-derivatives and Pheopigments group to the total
250 Chlorophyll *a* pool was calculated by dividing their concentrations by the $\Sigma_{\text{[Chlorophyll a]}}$
251 concentration, used as a proxy of biomass ($\Sigma_{\text{[Chlorophyll a]}}$ = [Chlorophyll *a*] + [Chlorophyll *a*-
252 derivatives] + [Pheopigments]). The de-epoxidation state (%), defined as the xanthophyll
253 ratio of Diatoxanthin to the Diadinoxanthin + Diatoxanthin pool, was calculated as
254 [Diatoxanthin]/([Diadinoxanthin] + [Diatoxanthin]) x100.
255 Additionally, pigment concentrations were used to reconstruct the microphytobenthic
256 community absorption spectrum for Qphar estimation, thus providing a more accurate
257 assessment of light actually absorbed by diatoms at the substrata surface during the high-
258 light treatment (supplementary Fig. 1B-E; see supplementary materials and methods).

259 Data treatment

260 Raw 18S rRNA gene amplicon sequencing data were processed via the SAMBA workflow to
261 generate amplicon sequence variants, which were assigned taxonomically with the PR2
262 (v5.0.0) database. Reads were normalized by coverage-based rarefaction and transformed
263 to relative abundances. Diversity between communities was tested using the Wilcoxon rank-
264 sum test.
265 For both communities, the net impact values of stress ($\Delta_{\text{After-Before}}$) on photophysiological
266 parameters were calculated and compared to those of dark-adapted control samples, which
267 accounts for metabolic drift over time, using Welch's two-sample t-test.
268 Pigment composition was analyzed using ANOSIM tests based on Euclidean distances
269 between individual coordinates. These were extracted from the first two axes of each PCA
270 performed on Hellinger-transformed pigment concentrations to assess the significant effects
271 of treatments and communities. A Between-Class Analysis was performed to characterize
272 the effects of the stress factor on the total inertia of pigment profiles for both communities. A
273 SIMPER analysis on relative proportions, performed independently for each sediment-
274 associated and sediment-free biofilm community, was used to identify pigments that varied
275 significantly under each stress compared to the dark-adapted control samples. Changes in
276 pigment ratios were tested using the Mann-Whitney U test.

RESULTS

Motile diatom *P. strigosum* dominates the eukaryotic microphytobenthic community

Despite inherent biases, such as the amplification of free eDNA or the underrepresentation of rare species in communities[48], the sequencing approach provided a relevant semi-quantitative overview of the biovolume-dominant eukaryotic microphytobenthic taxa. The two communities displayed distinct assemblages, with significantly lower diversity indices and reduced variability among sediment-free biofilm replicates compared with sediment-associated biofilms (Wilcoxon-Mann-Whitney, $P < 0.05$) (supplementary Fig. 2). The eukaryotic community was dominated by *Bacillariophyceae*, *Nematoda*, and *Arthropoda*, with an expected increase in the relative proportion of *Bacillariophyceae* in sediment-free biofilms, due to the substrata surface layer subsampling protocol which excluded much of the sediment-associated diversity (Fig. 1D). Autotrophic biovolume was largely dominated by the raphid species *Pleurosigma strigosum*, which accounted for 88.7% of sediment-free biofilm relative abundances, together with other benthic diatoms, such as the genera *Navicula* and *Gyrosigma* (possibly *G. balticum*[49]) (Fig. 1C, E).

Downward vertical migration triggered under the three stresses

Vertical migration was assessed by tracking F_0 measurements under the hydrogen peroxide-, plasma-, and high-light-induced ROS stresses. F_0 serves as a proxy for biomass, effectively reflecting the motile behavior of benthic diatoms[17]. Indeed, in sediment-free biofilm samples subjected to the hydrogen peroxide, plasma, and high-light treatments, F_0 levels did not decrease compared to dark-adapted control replicates (supplementary Tables 3 and 4). In addition, Fv/Fm values remained stable for the hydrogen peroxide and plasma treatments. Altogether, these results rule out potential Chlorophyll *a* bleaching and the induction of karyostrophy under any of the three stresses[32, 33].

Regardless of how ROS were produced or applied, the *P. strigosum* dominated biofilms sensed both metabolic and environmental oxidative stresses, responding with a marked downward migration (Fig. 2). This was quickly followed by a gradual recovery of surface biomass under all stresses as soon as the stress ended. The intensity of the behavioral response varied according to the type of stress, with exogenous ROS triggering the strongest effect. In particular, the hydrogen peroxide treatment induced a clear and rapid on/off switch-migration within approximately one minute (experimental observation), with a 75.5% decrease in F_0, followed by the plasma exposure causing a 35.6% decrease and an 8.9% reduction under the high-light stress (Table 2). Within this framework, the fastest return of biomass at the sediment surface occurred after the hydrogen peroxide exposure, with a

312 +116% F_0 min^{-1} recovery slope, compared with +67% under high-light and +47% after the
313 plasma stress, respectively.
314
315 ***Table 2. Extent of the behavioral response of the microphytobenthic surface biomass***
316 *Table reporting changes in F_0 (data from Fig. 2), at the sediment surface (average ± SD, arbitrary*
317 *unit), before and after treatments, for the sediment-associated biofilm samples (n = 8 for high-light and*
318 *cold atmospheric plasma; n = 5 for hydrogen peroxide). Dark-adapted control(1), (2), and (3) correspond*
319 *to samples measured in parallel to the high-light, hydrogen peroxide, and cold atmospheric plasma*
320 *experimental treatments, respectively. The Δ After-Before (a.u.) and Changes (%) columns summarize*
321 *the temporal evolution of surface F_0. The post-stress recovery slope is calculated using a linear*
322 *regression model applied to F_0 fluorescence kinetics over 60 minutes after stress cessation, as an*
323 *indicator of microphytobenthos resilience. The slope reflects the rate of F_0 variation per minute during*
324 *recovery (F_0 min^{-1}).*

Treatments	F_0 Before (a.u.)	F_0 After (a.u.)	Δ After-Before (a.u.)	Changes (%)	Recovery slope (F_0 min^{-1})
Dark-adapted control(1)	12752 (1606)	14540 (787)	+1788	**+14%**	**+11**
High-light	13080 (807)	11916 (993)	-1164	**-9%**	**+67**
Dark-adapted control(2)	11393 (1457)	12232 (703)	+839	**+7%**	**-2**
Hydrogen peroxide	11546 (1100)	2824 (433)	-8722	**-76%**	**+116**
Dark-adapted control(3)	15263 (726)	14906 (945)	-356	**-2%**	**+17**
Cold atmospheric plasma	15496 (843)	9979 (1801)	-5517	**-36%**	**+47**

325

326 Divergent photophysiology: Exogenous ROS oxidize pigments with limited 327 photosynthetic impairment vs. high-light-driven photoinhibition

328 To complement the finding that microphytobenthic vertical migration behavior may be
329 triggered by ROS, we assessed the metabolic cost associated with these stresses by
330 examining the functional response of the photosynthetic apparatus. To this end, key
331 photosynthetic parameters and lipophilic pigment data were monitored in both communities.
332 Unlike sediment-associated biofilms, the sediment-free biofilms capture the impact on the
333 most complete and intact community possible, as supported by the sequencing results,
334 without the possibility of mitigation through migratory responses.

335 Before stress exposure, all replicates across all treatments showed high initial Fv/Fm values
336 (> 0.67) and high initial α-slope values (> 0.32), indicating that the cells were in an optimal
337 physiological state. In both communities, post-exposure photosynthetic efficiency values
338 remained high under all three stresses. This was particularly true for exogenous stresses in
339 sediment-free biofilms, where despite the inability to mitigate stress through migration, the
340 cells maintained high Fv/Fm and α-slope values (> 0.66 and > 0.33, respectively). Taken
341 together, these results support that, as for the high-light treatment, the intensities of the
342 hydrogen peroxide and plasma stresses remained within the photophysiological tolerance
343 range of the cells despite their inability to migrate, thereby enabling reliable interpretation of
344 the data.
345 The sediment-associated biofilm community showed a general decrease in photosynthetic
346 efficiency under all three stresses, characterized by a significant drop in the α-slope and
347 Fv/Fm values (Welch's two-sample t-test, $P < 0.05$). An effective photoprotective response
348 was observed exclusively after the high-light exposure, with increases in NPQ^{1000} and
349 $Y(NPQ)^{1000}$ values, indicating controlled dissipation of excess energy (Fig. 3; supplementary
350 Fig. 3). Conversely, stress exposure in sediment-free biofilms revealed a marked
351 photophysiological impact only under the high-light treatment, with a drop in Fv/Fm values,
352 along with a strong activation of the effective photoprotection Y(NPQ) and an increase in
353 unregulated photoinhibition $Y(NO)_{m\ obs}$. The increase in this uncontrolled dissipation
354 component reflects an excess of irradiance absorbed by the cells under the high-light
355 treatment, estimated at ~519 µmol photons m^{-2} s^{-1} by Qphar and recalculated at ~448 µmol
356 photons m^{-2} s^{-1} when accounting for the cell pigment packaging effect. The hydrogen
357 peroxide and plasma exposures did not significantly alter the state of the photosynthetic
358 electron transport chain, as particularly evident when comparing the photosystem II quantum
359 yield response curves (Fig. 4). Nevertheless, the exogenous plasma stress appeared more
360 impactful than the hydrogen peroxide, highlighted by a decrease in $rETR_{m\ obs}$ in both
361 sediment-associated and sediment-free biofilm communities.
362
363 Microphytobenthic lipophilic pigment analyses revealed diatom-typical profiles in all samples,
364 with dark-adapted sediment-free biofilms providing the most representative unstressed
365 baseline composition: Chlorophyll *a* and its derivatives (58.3%), Fucoxanthin and its
366 derivatives (28%), Chlorophyll *c2* (6.7%), Diadinoxanthin + Diatoxanthin (2.4%), ββ + βε-
367 carotene (1.3%) (supplementary Fig. 4). Both communities were characterized by a clear
368 difference in their pigment compositions (ANOSIM, R = 1; P = 1e-04, supplementary Fig.
369 5A). This was due to higher relative proportions of Chlorophyll *a*, Fucoxanthin, and
370 Chlorophyll *c2* in sediment-free biofilms, whereas sediment-associated biofilm samples
371 exhibited an increase in degraded forms such as Pheopigments, Unknown-carotenoids, or

Fucoxanthin-like. Within both communities, stresses significantly affected pigment profiles (sediment-associated biofilms ANOSIM R = 0.82, *P* = 1e-04, supplementary Fig. 5B and sediment-free biofilms ANOSIM R = 0.73, *P* = 1e-04, supplementary Fig. 5C), which explain 84% and 67% of the total inertia observed in the sediment-associated and sediment-free biofilm samples, respectively (supplementary Fig. 6). SIMPER analyses revealed a stronger impact of exogenous stresses on pigment composition compared to the high-light stress in both communities, with a greater number of significantly affected pigments relative to dark-adapted control samples (SIMPER, $P < 0.05$). This was particularly evident in sediment-associated biofilm samples, where 3, 17, and 39 pigments were significantly affected by the high-light, hydrogen peroxide, and plasma treatments, respectively, compared to 10, 15, and 16 pigments for sediment-free biofilms. This differential impact of the stressors was mainly driven by Chlorophyll *a*-derivatives rather than Pheopigments (Fig. 5B, C), suggesting that the hydrogen peroxide and plasma exposures caused a broader and untargeted effect, with direct oxidation of numerous pigments despite short exposure times, whereas the high-light treatment represented a more targeted stress. The latter was particularly characterized by the activation of the xanthophyll cycle, with significant increases in the de-epoxidation state, especially in sediment-free biofilms, where the average ratio exceeded 46% (Fig. 5A, concentrations detailed in supplementary Table 5). Finally, sediment-free biofilms showed the same impact dynamics on Chlorophyll *a*-derivatives as sediment-associated biofilms, confirming that the stresses differentially affected the surface motile diatoms themselves.

DISCUSSION

High-light-induced vertical migration in microphytobenthos

Pigment profiles provided a chemotaxonomic signal typical of diatoms, characterized by high fucoxanthin content together with Chlorophyll *c2* and Chlorophyll *a*[28], which corroborated the sequencing results (Fig. 1E). Both communities were characterized by a biovolume dominated by benthic diatoms, especially *Pleurosigma strigosum*, along with other autotrophs and meiofauna (*e.g.* nematodes, copepods, and ostracods), corroborating previous microscopic observations[49] and literature on microphytobenthos in similar environments[50, 51]. In line with these observations, the motile behavioral response, pigmentary mobilization, and photophysiological signals can be largely attributed to the benthic diatoms dominating the surface biovolume, with *P. strigosum* playing a predominant role.

In sediment-associated biofilm experiments, exposure of the microphytobenthos to 1500 µmol photons m^{-2} s^{-1} for 30 minutes induced a moderate decrease in F_0, indicating a shift in biofilm dynamics from upward to downward migration (Fig. 2). This response was reversible,

407 with biomass returning to the surface after the treatment ended. Vertical migration in benthic
408 diatoms is governed by self-sustained circadian and tidal rhythms that require regular
409 resetting to remain synchronized[20, 52]. These rhythms are further modulated by
410 environmental cues, allowing rapid and temporally adjustable responses[18, 21, 23]. The
411 induction of a high-light-driven vertical migration strategy through muddy substrata was
412 expected and is well documented in many autotrophic microorganisms, including *P.*
413 *strigosum*, highlighting a relatively common evolutionary advantage[17, 20, 26]. To maintain
414 optimal cellular performance and cope with ROS, this migratory response operates in
415 synergy with other photoprotective mechanisms that collectively sustain cellular fitness[6].

416 Migration and photoprotection act synergistically under high-light-induced 417 ROS

418 In parallel to the downward migration, a decline in photosynthetic efficiency was observed in
419 the high-light-treated sediment-associated biofilm samples, suggesting that vertical migration
420 did not maintain short-term photosynthetic performance. This decline was likely caused by an
421 increase in Y(NPQ) due to targeted mobilization of the Diadinoxanthin-Diatoxanthin cycle
422 (Fig. 3 and 5A), combined with slight photoinhibition, consistent with previous reports[26, 53].
423 Irradiance is known to generate both endogenous and exogenous ROS-high-oxidative-
424 potential molecules that can cross membranes and act as signaling agents across multiple
425 subcellular compartments[6, 9, 54–59]. Diatoms must cope with them, as excessive
426 accumulation poses deleterious risks, including the oxidation of essential photosynthetic
427 components[10, 11]. To prevent ROS formation, high-light can rapidly trigger effective
428 Y(NPQ) supported by the Diadinoxanthin + Diatoxanthin xanthophyll pool, where
429 overstimulation of the photosynthetic electron transport chain induces lumen acidification,
430 upregulating the pH-sensitive diadinoxanthin de-epoxidase enzyme[15, 30, 60]. Here, both
431 vertical migration and xanthophyll cycle activation likely limit ROS production and
432 accumulation, indicating that all components of a typical and effective photoprotection
433 strategy are engaged, as expected for benthic intertidal diatoms under photooxidative stress.
434 In addition, diatoms actively regulate cellular redox balance under light-induced ROS via both
435 enzymatic and non-enzymatic antioxidant capacities, including upregulation of superoxide
436 dismutase and ascorbate peroxidase[37, 39, 61], mobilization of antioxidant non-protein
437 thiols and glutathione pools[62], or by direct ROS scavenging by carotenoids[29, 31, 38].
438 Although Chlorophyll *a* fluorescence is generally a reliable indicator of cellular physiological
439 state under various abiotic stresses[63], the presence of a sedimentary environment in
440 sediment-associated biofilm samples can alter the signal (*e.g.* cell reorientation, effective
441 light exposure, or downward migration, potentially leaving fewer viable cells at the surface).
442 Consequently, sediment-associated biofilms photosynthetic parameters must be interpreted

443 with caution[45, 64]. The sediment-free biofilms results help to overcome this potential bias,
444 thereby clarifying the synergy between the need for migration, the xanthophyll cycle
445 activation, and the photosynthetic efficiency. Cells from sediment-free biofilms, unable to
446 adjust their vertical position, displayed a stronger increase in the de-epoxidation state, as a
447 high-light-compensatory response (Fig. 5A). Enhanced xanthophyll cycle mobilization is a
448 well-described compensatory response in diatoms with impaired motility, as shown under
449 light exposure combined with latrunculin motility inhibitors[14, 26, 65]. In natural
450 environments, this trade-off becomes evident when examining the de-epoxidation state of
451 epipsammic diatoms, which inhabit brighter environments where vertical migration is limited,
452 resulting in a stronger response than in epipelic diatoms[65–67]. Despite the xanthophyll
453 cycle response in sediment-free biofilms, an increase in Y(NO) indicates that the stress still
454 induced a slight unregulated photoinhibition from the lowest irradiances of the light curves
455 (Fig. 4).
456 In fact, the high-light treatment induced finely tuned and metabolically controlled cellular
457 adjustments, involving subtle pigment remodeling as part of a photoprotective strategy, which
458 works in synergy with vertical migration behavior. However, although this targeted response
459 is likely driven by intracellular variations (e.g. metabolic imbalances resulting from ROS
460 accumulation primarily due to light, and potentially in combination with other stresses, such
461 as temperature, pH, exposure to toxic substances, or nutrient availability), migration may
462 also result from environmental oxidative signals[58]. These include exogenous high-light-
463 ROS generated by photooxidation of dissolved organic matter in muddy substrata[56, 58,
464 68], and ROS actively or passively released by neighboring cells in the biofilm, leading to
465 their local accumulation[13, 54, 69]. Moreover, precipitation can deliver water containing up
466 to 85 µM H_2O_2[58]. All these conditions in intertidal environments can rapidly and transiently
467 increase exogenous oxidative stress for microphytobenthos, an environmental scenario not
468 far from the hydrogen peroxide and plasma treatments, although these stresses involve
469 higher concentrations than those typically measured in tidal zones[56].

470 Exogenous ROS induce untargeted oxidative stress on diatoms

471 As for high-light-induced photooxidation, exogenous ROS generated by the hydrogen
472 peroxide and plasma stresses, including H_2O_2, likely interacted with sedimentary dissolved
473 organic matter, triggering chemical reactions. These reactions could alter oxidative
474 conditions in sediment samples, including potential acidification that may explain the
475 increase in the de-epoxidation state. This xanthophyll cycle activation in sediment-associated
476 biofilms appeared to occur without development of regulated Y(NPQ) (supplementary Fig. 3).
477 As previously discussed, downward vertical migration into the sediment can strongly interfere
478 with fluorescence measurements, including underestimation of NPQ[45, 64]. In addition,

479 migration of viable cells into deeper sediment layers may leave senescent or physiologically
480 impaired cells at the surface, further altering the residual fluorescence signal. This
481 interpretation is supported by the higher relative abundance of Pheopigments observed in
482 sediment-associated biofilms compared to sediment-free biofilm samples (Fig. 5C), along
483 with the increase in Y(NO), concomitant with the apparent loss of Y(NPQ) development
484 capacity. Due to the substantial downward migration of biomass, the reliability of surface
485 fluorescence measurements in sediment-associated biofilm samples is intrinsically
486 compromised, and it is therefore not possible to definitively conclude whether the observed
487 signal reflects a reduced and physiologically altered surface population or whether the
488 induced diatoxanthin is preferentially used in antioxidant functions rather than
489 photoprotective NPQ[38].
490 In fact, exogenous stresses in both communities exhibited a stronger untargeted oxidizing
491 capacity, leading to extensive and differential oxidation of the pigment system. The presence
492 of sediment, potentially creating altered oxidative conditions, combined with an associated
493 pool of degraded Pheopigments, could explain the higher Between-Class Analysis explained
494 inertia values observed for sediment-associated biofilms (Supplementary Fig. 6). The global
495 impact of the hydrogen peroxide and plasma treatments is particularly reflected in the
496 oxidation of Chlorophyll *a* into Chlorophyll *a*-derivatives (Fig. 5B), suggesting a random and
497 direct oxidation of lateral chains of Chlorophyll *a* molecules[70]. Some of these alternative
498 forms of Chlorophyll *a* may have cellular functions[9, 29, 71], and their accumulation may
499 serve as an indicator of environmental conditions[5]. Despite the plasma treatment inducing
500 a higher accumulation of Chlorophyll *a*-derivatives, indicating more detrimental conditions
501 than the hydrogen peroxide exposure, both exogenous stresses resulted in high post-stress
502 photosynthetic performance. This supports the relevance of the applied stress intensities, as
503 structural modifications in part of the Chlorophyll *a* pool did not prevent the maintenance of
504 light-harvesting functions, even when migration was impaired.

505 Vertical migratory behavior triggered by exogenous ROS

506 Our results showed that brief exposure to hydrogen peroxide and plasma-ROS had a
507 moderate impact on photophysiology (Fig. 4), while simultaneously triggering a rapid
508 downward vertical migration (Fig. 2). Reported migration velocities are highly variable,
509 typically ranging from 1 to 30 µm s^{-1} for horizontal movements, and generally lower for
510 vertical displacements, generally between 0.17 and 0.28 µm s^{-1} [17, 20, 21, 24]. Based on
511 these values, diatoms could theoretically migrate vertically by approximately 102 µm and 168
512 µm under our 10-minute stresses, reaching muddy layers where light availability is reduced
513 by ~66%[65], which is consistent with the strong decrease observed in F_0. In both cases,
514 stresses did not compromise the motility of diatoms, which rapidly initiated an upward

515 migration once the stresses ended, as shown by post-stress recovery slope (Table 2). This
516 plasticity in behavioral response, which adjusts in real time to changing surface conditions,
517 was nevertheless more affected under the plasma exposure, with a slower return of biomass,
518 suggesting a harsher stress. ROS, such as H_2O_2, are described in literature as secondary
519 messengers that mediate signal transduction and activate defense mechanisms during
520 adaptation to both biotic and abiotic stress[5, 6, 8, 59], including motile capacities in
521 microalgae[25, 55, 57, 72, 73]. The hypothesis that ROS are one of the components inducing
522 migration under a composite stress such as cold atmospheric plasma is corroborated by the
523 strong migration observed under the hydrogen peroxide positive control, which specifically
524 isolates the effect of H_2O_2. This molecule has been widely used in previous studies to
525 investigate its role as a driver in various cellular pathways in microalgae[59, 72, 74–77], as
526 exogenously applied H_2O_2 can accumulate intracellularly via transmembrane diffusion
527 through aquaporins[78]. The results presented here demonstrate its key role as a strong
528 on/off trigger of the transient motile response. Moreover, the behavioral response did not
529 reflect the impact of exogenous stresses on the pigment system, as the strongest
530 mobilization occurred under the hydrogen peroxide treatment rather than under plasma.
531 Together, these results suggest that vertical migration could be triggered by ROS, especially
532 H_2O_2, without necessarily being associated with a decline in photosynthetic performance. In
533 other words, the presence of ROS, even in darkness and without impaired photosynthetic
534 capacity, is sufficient to trigger downward motility. This triggering of migration occurs without
535 inducing an effective controlled photoacclimatory Y(NPQ) response involving the xanthophyll
536 cycle. Exogenous ROS likely acted through a sophisticated signal transduction network to
537 trigger this rapid and essential motility response of the microphytobenthos under harmful
538 oxidative environmental conditions[6, 8]. The precise cellular pathways by which H_2O_2 act,
539 either directly or indirectly, to trigger this behavior remain uncertain in benthic diatoms and
540 require further investigation. Nevertheless, certain studies in the literature provide a solid
541 foundation for preliminary research.

542 Do ROS induce calcium signaling underlying motility?

543 In benthic pennate diatoms, gliding motility is driven by an actin-based cytoskeletal system
544 organized along the apical axis. This system transmits force through transmembrane
545 complexes to mucopolysaccharide microfibrils secreted via the raphe slit, thereby enabling
546 adhesion and traction on substrata[20, 22]. ROS can plausibly act on several components of
547 the gliding system, including cytoskeletal reorganization, adhesive mucilaginous compounds,
548 ATP availability, gene expression, or by generating oxidized metabolites that function as
549 infochemicals and secondary messengers in specific signaling pathways (*e.g.* oxylipins, thiol
550 compounds)[12, 22, 79–83]. Nevertheless, a migration behavior primarily controlled by ROS-

551 calcium signaling remains one of the most prominent hypotheses, both of them being central
552 components of microalgal adaptation to environmental stressors[84].
553 Recent studies have shown that disruption of the transthylakoid proton gradient inhibits
554 motility in benthic diatoms, potentially through effects on calcium homeostasis, thereby
555 suggesting a broader link between behavior and high light-driven photoprotection[77, 85].
556 Our results provide experimental evidence that diatom migration can be triggered in
557 darkness and independently of an effective Y(NPQ) response, further refining the regulatory
558 cascade underlying this behavior by linking ROS to an "oxidotactic" motility that may involve
559 calcium signaling. Elevations of stromal Ca^{2+} have been reported in response to intracellular
560 ROS accumulation under high light and after exogenous H_2O_2 exposure[76, 77]. In plants,
561 both endogenous H_2O_2 accumulation and exogenous H_2O_2 exposure induce Ca^{2+} influx via
562 calcium channel activation[86], an influx implicated in controlling diatom migration[87, 88]
563 and, more recently, contributing to gliding motility through EukCatAs ion channels that
564 regulate cytosolic Ca^{2+} levels[89]. In addition, it has been shown that certain membrane
565 receptor kinases can directly sense extracellular H_2O_2 and initiate Ca^{2+} channel opening
566 without a prior intracellular H_2O_2 accumulation[90]. In the environment, exposure to copper
567 promotes oxidative stress and intracellular Ca^{2+} perturbations alongside active gliding
568 motility[25], and new evidence has identified a bistability in phytoplanktonic microalgae, in
569 which vertical migration switches are driven by a ROS-induced oxidative stress threshold[72].
570
571 Our study does not provide a definitive conclusion on the full role of ROS, such as H_2O_2.
572 Nevertheless, these results, supported by recent literature, help to identify the major putative
573 components underlying the cellular signaling of this behavior (Fig. 6). Although detailed
574 information on the ROS-Calcium-Motility interplays is still lacking, particularly regarding how
575 the calcium acts on the locomotion machinery pathways, we propose that certain rapid
576 responses to environmental cues, such as a vertical migratory behavior switch observed in
577 this experiment, are mediated, at least in part, by a ROS-sensing system.

578 CONCLUSION

579 All results provide strong evidence for the key role of ROS, particularly H_2O_2, as a critical
580 signaling molecule triggering the rapid motile behavior in diatom-dominated
581 microphytobenthic biofilms. The strongest downward migration occurred under exogenous
582 stresses that minimally impacted photosynthetic efficiency, despite a broad and untargeted
583 oxidative stress on pigments. Moreover, these exogenous stresses were unable to induce an
584 effective, controlled photoprotective response, as reflected by Y(NPQ). This demonstrates
585 that exposure to H_2O_2 alone, in the absence of any light cue, is sufficient to trigger a plastic

motility. Such a response suggests a signaling pathway that may operate independently from those governing photophysiology, thereby broadening the ecological relevance of vertical migration in a multi-stress environmental context. This stress-mitigation strategy can act synergistically with pigments under high irradiance in natural environments, as supported by the enhanced activation of the xanthophyll cycle when migration was restricted. Together, the findings corroborate previous studies showing that vertical migration is an important adaptive trait allowing diatoms to regulate homeostasis and support long-term physiological performance.

By demonstrating the importance of ROS sensing in shaping microphytobenthic motility, these results indicate that benthic diatoms are able to monitor both metabolic and environmental ROS. This ROS-mediated early warning sensing system likely represents an adaptive strategy that enables efficient surveillance of environmental conditions, allowing cells to rapidly prevent deleterious conditions, maintain cellular fitness, and ultimately support the ecological success of diatoms in highly variable environments. This offers new insights into how oxidative stress regulates autotrophic life and more broadly highlights its key role within the aquatic microbiome. The response to oxidative challenges likely relies on a complex signaling cascade that requires further in-depth investigation to identify potential effectors in ROS-motility signaling and clarify how triggering this behavior allows cells to cope with oxidative stress in natural environments.

ACKNOWLEDGMENTS

Our thanks go to Johann Lavaud for his valuable discussions on photophysiology. We are also thankful to Manon Leroux for her essential assistance in the laboratory during the experiment. We acknowledge the chromatography and mass spectrometry facility at the Concarneau Marine Station (PtSMB-MNHN) for providing access to the HPLC.

CONFLICTS OF INTEREST

The authors declare no conflict of interest.

FUNDING

This work was funded by the Institut de l’Océan from the Sorbonne University alliance and the Muséum national d’Histoire naturelle.

DATA AVAILABILITY

All scripts used to generate the figures and perform the analyses are available on GitHub, and are also archived on Zenodo. The datasets generated and analyzed during the current study are available in the Zenodo repository. The raw sequencing data have been deposited in the European Nucleotide Archive (ENA) under project accession number **ERA33152396** (Experiments **ERX14500286 – ERX14500369**; Runs **ERR15095684 – ERR15095767**) and can be accessed via the ENA portal. The raw chromatogram files used for pigment analyses are available in the Zenodo repository.

AUTHOR CONTRIBUTIONS

AD: Conceptualization, Methodology, Investigation, Data curation, Formal analysis, Visualization, Writing - original draft. BJ: Data curation, Formal analysis, Validation, Writing - review & editing. TR: Data curation, Methodology, Formal analysis. TD: Resources, Methodology, Writing - review & editing. CH: Supervision, Methodology, Data curation, Formal analysis, Validation, Writing - review & editing.

REFERENCES

1. Kühl M, Jorgensen BB. The light field of microbenthic communities: radiance distribution and microscale optics of sandy coastal sediments. *Limnol Oceanogr* 1994;39:1368–1398. 10.4319/lo.1994.39.6.1368
2. Underwood GJC. Microphytobenthos. Encyclopedia of Ocean Sciences. Academic Press, 2001, 1770–1777. 10.1006/rwos.2001.0213
3. Pinckney JL. A mini-review of the contribution of benthic microalgae to the ecology of the continental shelf in the South Atlantic Bight. *Estuaries coast* 2018;41:2070–2078. 10.1007/s12237-018-0401-z
4. Hubas C, Passarelli C, Paterson DM. Microphytobenthic biofilms: composition and interactions. In: Beninger PG (ed.), Mudflat Ecology. Cham: Springer International Publishing, 2018, 63–90. 10.1007/978-3-319-99194-8_4
5. Waszczak C, Carmody M, Kangasjarvi J. Reactive oxygen species in plant signaling. *Annu Rev Plant Biol* 2018;69:209–236. 10.1146/annurev-arplant-042817-040322

643 6. Falciatore A, Mock T (eds). The molecular life of diatoms. Cham: Springer International
644 Publishing, 2022. 10.1007/978-3-030-92499-7
645 7. Duchêne C et al. Diatom phytochromes integrate the underwater light spectrum to sense
646 depth. *Nature* 2025;637:691–697. 10.1038/s41586-024-08301-3
647 8. Lepetit B, Dietzel L. Light signaling in photosynthetic eukaryotes with 'green' and 'red'
648 chloroplasts. *Environ Exp Bot* 2015;114:30–47. 10.1016/j.envexpbot.2014.07.007
649 9. Foyer CH, Hanke G. ROS production and signalling in chloroplasts: cornerstones and
650 evolving concepts. *Plant J* 2022;111:642–661. 10.1111/tpj.15856
651 10. Doose C et al. Non-enzymatic oxylipin production in a mudflat microphytobenthic biofilm:
652 evidence of a diatom response to light. *Front Photobiol* 2024;2:1441713.
653 10.3389/fphbi.2024.1441713
654 11. Nishiyama Y, Allakhverdiev SI, Murata N. A new paradigm for the action of reactive
655 oxygen species in the photoinhibition of photosystem II. *Biochim Biophys Acta Bioenerg*
656 2006;1757:742–749. 10.1016/j.bbabio.2006.05.013
657 12. Knieper M, Viehhauser A, Dietz K-J. Oxylipins and reactive carbonyls as regulators of the
658 plant redox and reactive oxygen species network under stress. *Antioxidants*
659 2023;12:814. 10.3390/antiox12040814
660 13. Mittler R et al. ROS signaling: the new wave? *Trends Plant Sci* 2011;16:300–309.
661 10.1016/j.tplants.2011.03.007
662 14. Serôdio J et al. Efficiency of photoprotection in microphytobenthos: role of vertical
663 migration and the xanthophyll cycle against photoinhibition. *Aquat Microb Ecol*
664 2012;16:161–175. 10.3354/ame01591
665 15. Blommaert L. Photoprotection in intertidal benthic diatoms. 2017;Ph.D. dissertation.
666 Ghent University. Faculty of Sciences, Ghent, Belgium.
667 16. Fauvel P, Bohn G. Le rythme des marées chez les diatomées littorales. *CR Soc Biol*
668 1907;62:121–123.

669 17. Consalvey M, Paterson DM, Underwood GJC. The ups and downs of life in a benthic
670 biofilm: migration of benthic diatoms. *Diatom Res* 2004;19:181–202.
671 10.1080/0269249X.2004.9705870
672 18. Coelho H, Vieira S, Serôdio J. Endogenous versus environmental control of vertical
673 migration by intertidal benthic microalgae. *Eur J Phycol* 2011;46:271–281.
674 10.1080/09670262.2011.598242
675 19. Barnett A et al. The vertical migratory rhythm of intertidal microphytobenthos in sediment
676 depends on the light photoperiod, intensity, and spectrum: evidence for a positive effect
677 of blue wavelengths. *Front Mar Sci* 2020;7:212. 10.3389/fmars.2020.00212
678 20. Cohn S, Manoylov K, Gordon R (eds). Diatom Gliding Motility. John Wiley & Sons, 2021.
679 10.1002/9781119526483
680 21. Morelle J et al. The photoprotective behavior of a motile benthic diatom as elucidated
681 from the interplay between cell motility and physiological responses to a light
682 microgradient using a novel experimental setup. *Microb Ecol* 2024;87:40.
683 10.1007/s00248-024-02354-7
684 22. Poulsen NC et al. Diatom gliding is the result of an actin-myosin motility system. *Cell*
685 *Motil Cytoskeleton* 1999;44:23–33. 10.1002/(SICI)1097-0169(199909)44:1%3C23::AID-
686 CM2%3E3.0.CO;2-D
687 23. Perkins R et al. Vertical cell movement is a primary response of intertidal benthic biofilms
688 to increasing light dose. *Mar Ecol Prog Ser* 2010;416:93–103. 10.3354/meps08787
689 24. Marques Da Silva J, Duarte B, Utkin AB. Travelling expenses: the energy cost of diel
690 vertical migrations of epipelic microphytobenthos. *Front Mar Sci* 2020;7:433.
691 10.3389/fmars.2020.00433
692 25. Suzuki S et al. Rapid transcriptomic and physiological changes in the freshwater pennate
693 diatom *Mayamaea pseudoterrestris* in response to copper exposure. *DNA Res*
694 2022;29:dsac037. 10.1093/dnares/dsac037

26. Morelle J et al. Inter-specific variability in photophysiological responses of epipelic diatoms to the actin inhibitor Latrunculin B. *Diatom Res* 2025;40:133–146. 10.1080/0269249X.2024.2447333
27. Nakov T, Beaulieu JM, Alverson AJ. Accelerated diversification is related to life history and locomotion in a hyperdiverse lineage of microbial eukaryotes (Diatoms, Bacillariophyta). *New Phytol* 2018;219:462–473. 10.1111/nph.15137
28. Roy S et al. (eds). Phytoplankton pigments: characterization, chemotaxonomy and applications in oceanography. Cambridge University Press, 2011. 10.1017/CBO9780511732263
29. Kuczynska P, Jemiola-Rzeminska M, Strzalka K. Photosynthetic pigments in diatoms. *Mar Drugs* 2015;13:5847–5881. 10.3390/md13095847
30. Goss R, Jakob T. Regulation and function of xanthophyll cycle-dependent photoprotection in algae. *Photosynth Res* 2010;106:103–122. 10.1007/s11120-010-9536-x
31. Latowski D, Kuczyńska P, Strzałka K. Xanthophyll cycle – a mechanism protecting plants against oxidative stress. *Redox Rep* 2011;16:78–90. 10.1179/174329211X13020951739938
32. Bastos A et al. Light response of karyostrophy in the benthic pennate diatom *Pleurosigma strigosum* (Bacillariophyceae): a complimentary photoprotective process? *J Phycol* 2025;61:1140–1152. 10.1111/jpy.70055
33. Furukawa T, Watanabe M, Shihira-Ishikawa I. Green- and blue-light-mediated chloroplast migration in the centric diatomPleurosira laevis. *Protoplasma* 1998;203:214–220. 10.1007/BF01279479
34. Jönsson B, Sundbäck K, Nilsson C. An upright life-form of an epipelic motile diatom: on the behaviour of *Gyrosigma balticum*. *Eur J Phycol* 1994;29:11–15. 10.1080/09670269400650421

721 35. Jesus B et al. Microscale imaging sheds light on species-specific strategies for photo-
722 regulation and photo-acclimation of microphytobenthic diatoms. *Environ Microbiol*
723 2023;25:3087–3103. 10.1111/1462-2920.16499
724 36. De Tommasi E et al. Multiple-pathways light modulation in *Pleurosigma strigosum* bi-
725 raphid diatom. *Sci Rep* 2024;14:6476. 10.1038/s41598-024-56206-y
726 37. Nymark M et al. An integrated analysis of molecular acclimation to high light in the
727 marine diatom *Phaeodactylum tricornutum*. *PLoS ONE* 2009;4:e7743.
728 10.1371/journal.pone.0007743
729 38. Lepetit B et al. Evidence for the existence of one antenna-associated, lipid-dissolved and
730 two protein-bound pools of diadinoxanthin cycle pigments in diatoms. *Plant Physiol*
731 2010;154:1905–1920. 10.1104/pp.110.166454
732 39. Valle KC et al. System responses to equal doses of photosynthetically usable radiation of
733 blue, green, and red Light in the marine diatom *Phaeodactylum tricornutum*. *PLoS ONE*
734 2014;9:e114211. 10.1371/journal.pone.0114211
735 40. Walpersdorf E et al. In situ oxygen dynamics and carbon turnover in an intertidal
736 sediment (Skallingen, Denmark). *Mar Ecol Prog Ser* 2017;566:49–65.
737 10.3354/meps12016
738 41. Stoeck T et al. Multiple marker parallel tag environmental DNA sequencing reveals a
739 highly complex eukaryotic community in marine anoxic water. *Mol Ecol* 2010;19:21–31.
740 10.1111/j.1365-294X.2009.04480.x
741 42. Eilers PHC, Peeters JCH. A model for the relationship between light intensity and the
742 rate of photosynthesis in phytoplankton. *Ecol Modell* 1988;42:199–215. 10.1016/0304-
743 3800(88)90057-9
744 43. Silsbe GM, Kromkamp JC. Modeling the irradiance dependency of the quantum
745 efficiency of photosynthesis. *Limnol Oceanogr Methods* 2012;10:645–652.
746 10.4319/lom.2012.10.645

44. Barranguet, Kromkamp J. Estimating primary production rates from photosynthetic electron transport in estuarine microphytobenthos. *Mar Ecol Prog Ser* 2000. doi:10.3354/meps204039
45. Consalvey M et al. PAM fluorescence: a beginners guide for benthic diatoms. *Diatom Res* 2005;20:1–22. 10.1080/0269249X.2005.9705619
46. Christof Klughammer, Ulrich Schreiber. Complementary PS II quantum yields calculated from simple fluorescence parameters measured by PAM fluorometry and the saturation pulse method. *PAM Application Notes* 2008;1:27–35.
47. Brotas V, Plante-Cuny M-R. The use of HPLC pigment analysis to study microphytobenthos communities. *Acta Oecol* 2003;24:S109–S115. 10.1016/S1146-609X(03)00013-4
48. Van Der Loos LM, Nijland R. Biases in bulk: DNA metabarcoding of marine communities and the methodology involved. *Mol Ecol* 2021;30:3270–3288. 10.1111/mec.15592
49. Gaubert-Boussarie J, Prado S, Hubas C. An untargeted metabolomic approach for microphytobenthic biofilms in intertidal mudflats. *Front Mar Sci* 2020;7:250. 10.3389/fmars.2020.00250
50. Underwood GJC, Barnett, M. What determines species composition in microphytobenthic biofilms. *Royal Netherlands Academy of Arts and Sciences* 2006;123–140.
51. Méléder V et al. Spatiotemporal changes in microphytobenthos assemblages in a macrotidal flat (Bourgneuf Bay,France). *J Phycol* 2007;43:1177–1190. 10.1111/j.1529-8817.2007.00423.x
52. Farré EM. The brown clock: circadian rhythms in stramenopiles. *Physiol Plant* 2020;169:430–441. 10.1111/ppl.13104
53. Prins A et al. Effect of light intensity and light quality on diatom behavioral and physiological photoprotection. *Front Mar Sci* 2020;7:203. 10.3389/fmars.2020.00203
54. Schneider RJ et al. Species-level variability in extracellular production rates of reactive oxygen species by diatoms. *Front Chem* 2016;4:5. 10.3389/fchem.2016.00005

774 55. Richter PR et al. High light-induced sign change of gravitaxis in the flagellate *euglena*
775 *gracilis* is mediated by reactive oxygen species. *Acta Protozool* 2003;42:197–204.
776 56. Abele-Oeschger D, Tüg H, Röttgers R. Dynamics of UV-driven hydrogen peroxide
777 formation on an intertidal sandflat. *Limnol Oceanogr* 1997;42:1406–1415.
778 10.4319/lo.1997.42.6.1406
779 57. Kottuparambil S et al. UV-B affects photosynthesis, ROS production and motility of the
780 freshwater flagellate, *Euglena agilis* Carter. *Aquat Toxicol* 2012;122–123:206–213.
781 10.1016/j.aquatox.2012.06.002
782 58. Morris JJ, Rose AL, Lu Z. Reactive oxygen species in the world ocean and their impacts
783 on marine ecosystems. *Redox Biol* 2022;52:102285. 10.1016/j.redox.2022.102285
784 59. Mizrachi A et al. Light-dependent single-cell heterogeneity in the chloroplast redox state
785 regulates cell fate in a marine diatom. *eLife* 2019;8:e47732. 10.7554/eLife.47732
786 60. Lavaud J et al. Influence of the diadinoxanthin pool size on photoprotection in the marine
787 planktonic diatom *Phaeodactylum tricornutum*. *Plant Physiol* 2002;129:1398–1406.
788 10.1104/pp.002014
789 61. Waring J et al. Light-induced responses of oxygen photoreduction, reactive oxygen
790 species production and scavenging in two diatom species. *J Phycol* 2010;46:1206–1217.
791 10.1111/j.1529-8817.2010.00919.x
792 62. Rijstenbil JW. UV- and salinity-induced oxidative effects in the marine diatom
793 *Cylindrotheca closterium* during simulated emersion. *Mar Biol* 2005;147:1063–1073.
794 10.1007/s00227-005-0015-4
795 63. Kalaji HM et al. Chlorophyll a fluorescence as a tool to monitor physiological status of
796 plants under abiotic stress conditions. *Acta Physiol Plant* 2016;38:102. 10.1007/s11738-
797 016-2113-y
798 64. Jesus B et al. Effects of vertical migrations by benthic microalgae on fluorescence
799 measurements of photophysiology. *Mar Ecol Prog Ser* 2006;315:55–66.
800 10.3354/meps315055

801 65. Cartaxana P et al. Physiological versus behavioral photoprotection in intertidal epipelic
802 and epipsammic benthic diatom communities. *J Exp Mar Biol Ecol* 2011;405:120–127.
803 10.1016/j.jembe.2011.05.027
804 66. Jesus B et al. Adaptations of microphytobenthos assemblages to sediment type and tidal
805 position. *Cont Shelf Res* 2009;29:1624–1634. 10.1016/j.csr.2009.05.006
806 67. Barnett A et al. Growth form defines physiological photoprotective capacity in intertidal
807 benthic diatoms. *ISME J* 2015;9:32–45. 10.1038/ismej.2014.105
808 68. Cheng K et al. Probing the photochemical formation of hydroxyl radical from dissolved
809 organic matter: insights into the H_2O_2-dependent pathway. *Environ Sci Technol*
810 2025;59:2245–2256. 10.1021/acs.est.4c10348
811 69. Diaz JM, Plummer S. Production of extracellular reactive oxygen species by
812 phytoplankton: past and future directions. *J Plankton Res* 2018;40:655–666.
813 10.1093/plankt/fby039
814 70. Amorim DS et al. Effects of cold plasma on chlorophylls, carotenoids, anthocyanins, and
815 betalains. *Food Res Int* 2023;167:112593. 10.1016/j.foodres.2023.112593
816 71. Ataka R et al. Determination of *N*-centered stereochemistry in N22-methylated
817 chlorophyll-*a* derivatives and their epimer-dependent optical spectra. *Chirality*
818 2024;36:e23681. 10.1002/chir.23681
819 72. Carrara F et al. Bistability in oxidative stress response determines the migration behavior
820 of phytoplankton in turbulence. *Proc Natl Acad Sci USA* 2021;118:e2005944118.
821 10.1073/pnas.2005944118
822 73. De Carpentier F et al. How abiotic stress-induced socialization leads to the formation of
823 massive aggregates in *Chlamydomonas*. *Plant Physiol* 2022;190:1927–1940.
824 10.1093/plphys/kiac321
825 74. Li Z et al. Common environmental stress responses in a model marine diatom. *New*
826 *Phytol* 2023;240:272–284. 10.1111/nph.19147

827 75. Volpert A et al. Diurnal fluctuations in chloroplast GSH redox state regulate susceptibility
828 to oxidative stress and cell fate in a bloom-forming diatom. *J Phycol* 2018;54:329–341.
829 10.1111/jpy.12638
830 76. Pivato M et al. Compartment-specific Ca^{2+} imaging in the green alga *Chlamydomonas*
831 *reinhardtii* reveals high light-induced chloroplast Ca^{2+} signatures. *New Phytol*
832 2023;240:258–271. 10.1111/nph.19142
833 77. Flori S et al. Diatoms exhibit dynamic chloroplast calcium signals in response to high light
834 and oxidative stress. *Plant Physiol* 2025;197:kiae591. 10.1093/plphys/kiae591
835 78. Bienert GP, Chaumont F. Aquaporin-facilitated transmembrane diffusion of hydrogen
836 peroxide. *Biochim Biophys Acta Gen Subj* 2014;1840:1596–1604.
837 10.1016/j.bbagen.2013.09.017
838 79. Pohnert G. Phospholipase A2 Activity Triggers the Wound-Activated Chemical Defense
839 in the Diatom *Thalassiosira rotula*. *Plant Physiol* 2002;129:103–111. 10.1104/pp.010974
840 80. Vardi A et al. A stress surveillance system based on calcium and nitric oxide in marine
841 diatoms. *PLoS Biol* 2006;4:e60. 10.1371/journal.pbio.0040060
842 81. Mukai K et al. Effects of light and hydrogen peroxide on gene expression of newly
843 identified antioxidant enzymes in the harmful algal bloom species *Chattonella marina*.
844 *Eur J Phycol* 2019;54:393–403. 10.1080/09670262.2019.1576062
845 82. Osuna-Cruz CM et al. The *Seminavis robusta* genome provides insights into the
846 evolutionary adaptations of benthic diatoms. *Nat Commun* 2020;11:3320.
847 10.1038/s41467-020-17191-8
848 83. Russo MT et al. The first genetic engineered system for ovothiol biosynthesis in diatoms
849 reveals a mitochondrial localization for the sulfoxide synthase OvoA. *Open Biol*
850 2023;13:220309. 10.1098/rsob.220309
851 84. Bowler C, Fluhr R. The role of calcium and activated oxygens as signals for controlling
852 cross-tolerance. *Trends Plant Sci* 2000;5:241–246. 10.1016/S1360-1385(00)01628-9

853 85. Morelle J et al. Light induced transthylakoidal proton gradient is a key signal driving the
854 downward migration of motile diatoms in sediments. *Sci Rep* 2025;15:20664.
855 10.1038/s41598-025-07737-5
856 86. Pei Z-M et al. Calcium channels activated by hydrogen peroxide mediate abscisic acid
857 signalling in guard cells. *Nature* 2000;406:731–734. 10.1038/35021067
858 87. Cooksey B, Cooksey KE. Calcium is necessary for motility in the diatom *Amphora*
859 *coffeaeformis*. *Plant Physiol* 1980;65:129–131. 10.1104/pp.65.1.129
860 88. McLachlan DH et al. Calcium release from intracellular stores is necessary for the
861 photophobic response in the benthic diatom *Navicula perminuta (Bacillariophyceae)*. *J*
862 *Phycol* 2012;48:675–681. 10.1111/j.1529-8817.2012.01158.x
863 89. Helliwell KE et al. Alternative mechanisms for fast Na+/Ca2+ signaling in eukaryotes via
864 a novel class of single-domain voltage-gated channels. *Curr Biol* 2019;29:1503-1511.e6.
865 10.1016/j.cub.2019.03.041
866 90. Wu F et al. Hydrogen peroxide sensor HPCA1 is an LRR receptor kinase in *Arabidopsis*.
867 *Nature* 2020;578:577–581. 10.1038/s41586-020-2032-3
868

869 SUPPLEMENTARY DATA

870 Two additional documents: (1) supplementary materials and methods and (2) supplementary
871 data.

FIGURE CAPTIONS

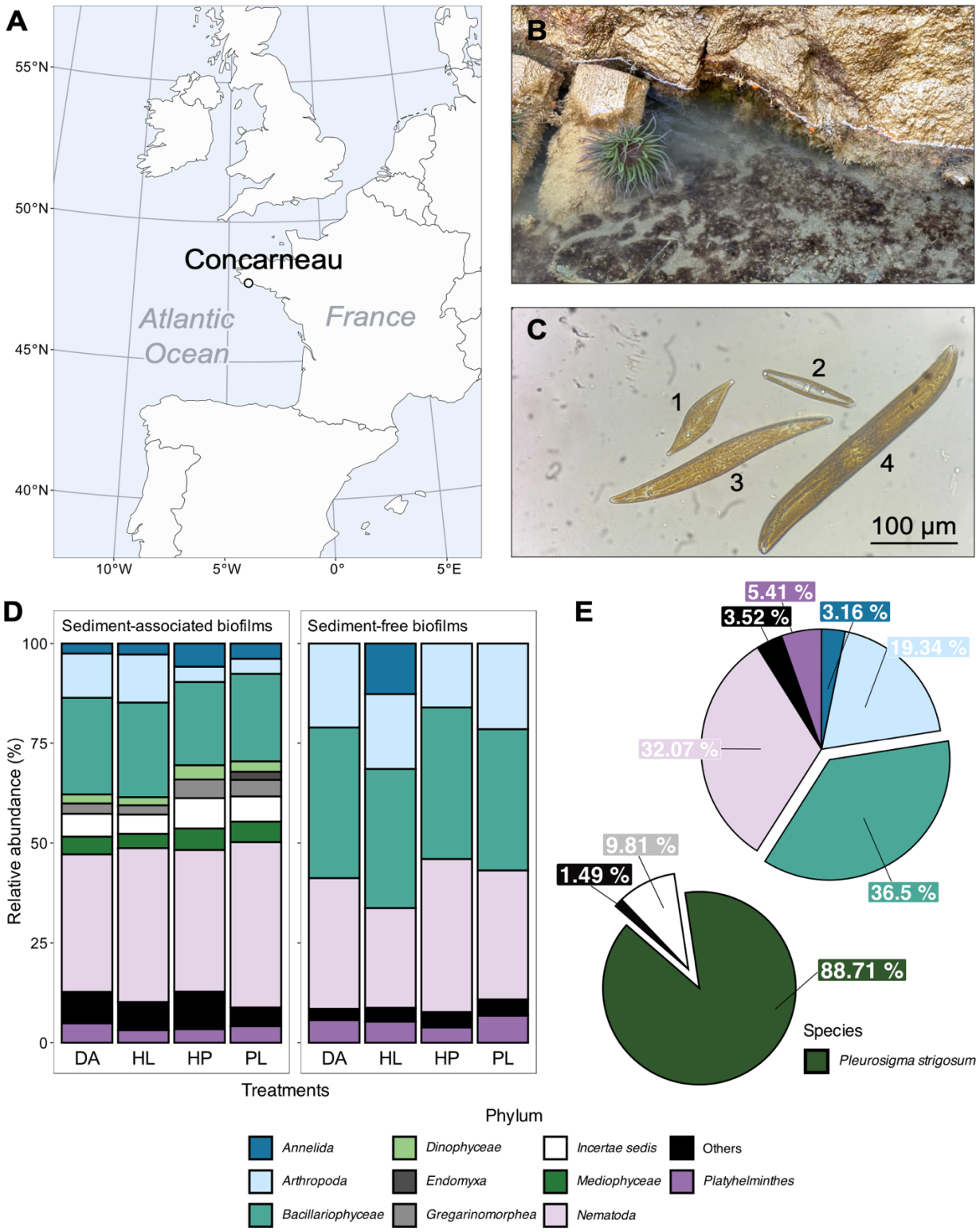

Figure 1. Microphytobenthic community diversity

A. *Geographical location of the studied microphytobenthic biofilm;* ***B.*** *Microphytobenthic biofilm (brown patches) developing on muddy substrata of the breeding pond;* ***C.*** *Light microscopy image of the most*

commonly observed diatom species in the microphytobenthic community: 1. Pleurosigma sp.*, 2. Navicula* sp.*, 3. Pleurosigma strigosum, 4. Gyrosigma* sp.*;* ***D.*** *Relative average abundance barplots (%; n = 5 per treatment) of eukaryotic phyla from microphytobenthic samples (some sequences derive from planktonic eDNA, thus contributing to the observed community composition) for sediment-associated and sediment-free biofilms, under Dark-Adapted control (DA), High-Light (HL), Hydrogen Peroxide (HP), and Cold Atmospheric Plasma (PL) treatments;* ***E.*** *Average sediment-free microphytobenthic biofilm community across all treatments, highlighting the prevalence of the autotrophic phylum Bacillariophyceae (first pie chart), and the significant contribution of Pleurosigma strigosum within Bacillariophyceae abundances (second pie chart). The "Others" category includes the sum of taxa with <2% abundance.*

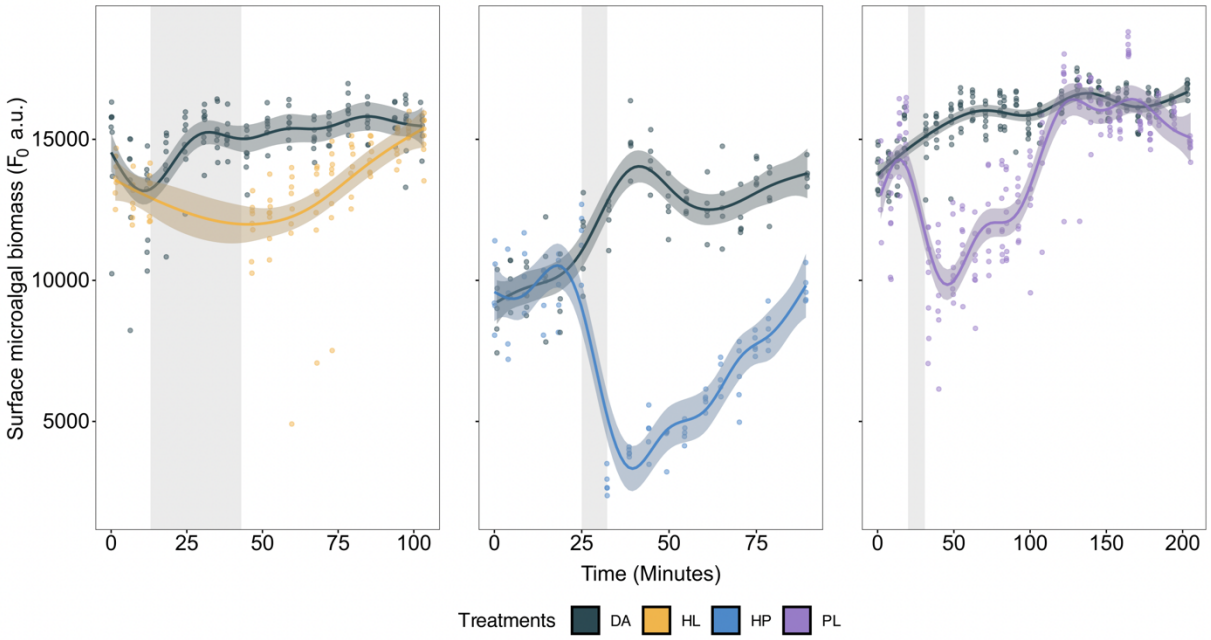

Figure 2. Downward migration of microphytobenthos under the three oxidative stresses
Temporal monitoring of surface microalgal biomass (F_0, arbitrary unit) for sediment-associated biofilms under the three oxidative stresses: High-Light (HL; n = 8), Hydrogen Peroxide (HP; n = 5), and Cold Atmospheric Plasma (PL; n = 8), compared to Dark-Adapted control biofilms (DA). Shaded grey areas indicate the stress period. All measurements were taken in the morning, during the upward migration phase of microphytobenthos.

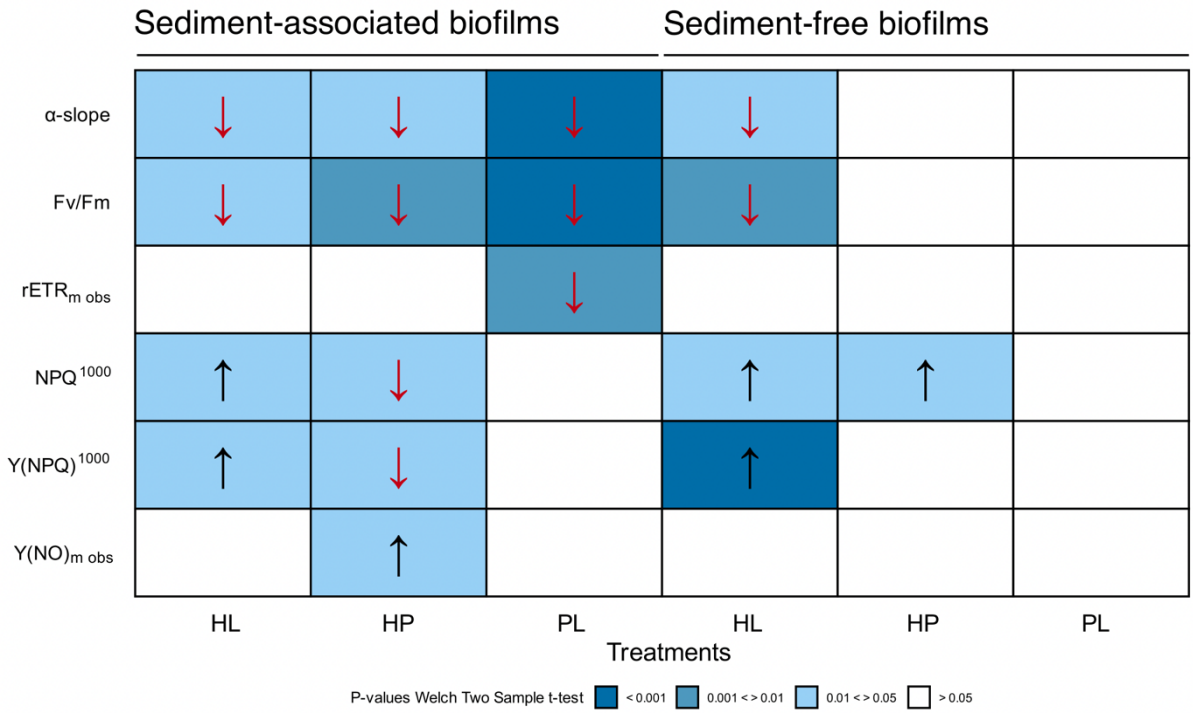

Figure 3. Heatmap of net photophysiological responses under oxidative stresses

Net impact of High-Light (HL), Hydrogen Peroxide (HP), and Cold Atmospheric Plasma (PL) treatments on photosynthetic parameters. Welch's two-sample t-test (n = 3) was used to calculate the stress-induced changes $\Delta_{After - Before}$, relative to dark-adapted control samples ($\Delta_{After - Before\ DA}$), in order to correct for the natural photophysiological variation observed under the darkness treatment. Arrows indicate the direction of the change induced by each stressor compared to dark-adapted control biofilms. α-slope (arbitrary unit). Fv/Fm (unitless) corresponds to the maximum quantum yield of photosystem II photochemistry under dark-adapted state. $rETR_{m\ obs}$ (arbitrary unit) and $Y(NO)_{m\ obs}$ (unitless) refer to the maximum values observed within the measured light curve range (without extrapolation). NPQ^{1000} (unitless) and $Y(NPQ)^{1000}$ (unitless) correspond to the maximum values measured after the final one-minute light curve step at 1000 µmol photons m^{-2} s^{-1} (without extrapolation). All fluorescence measurements were performed on dark-adapted samples for both sediment-associated and sediment-free biofilm communities. See supplementary Table 3 and 4 for detailed values.

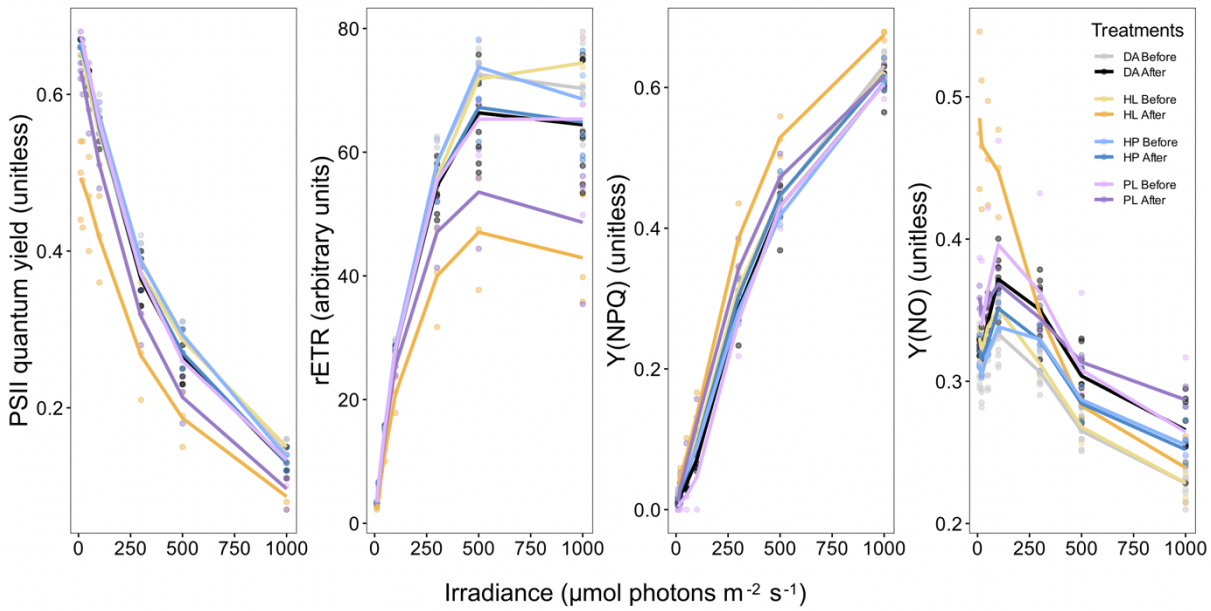

Figure 4. Photosynthetic efficiency profiles under treatments

Photosystem II (PSII) quantum yield (unitless), rETR (arbitrary unit), Y(NPQ) (unitless), and Y(NO) (unitless) response curves of sediment-free biofilm community, under the three stresses: High-Light (HL), Hydrogen Peroxide (HP), and Cold Atmospheric Plasma (PL), compared to Dark-Adapted control biofilms (DA). All photosynthetic parameters measured with n = 3.

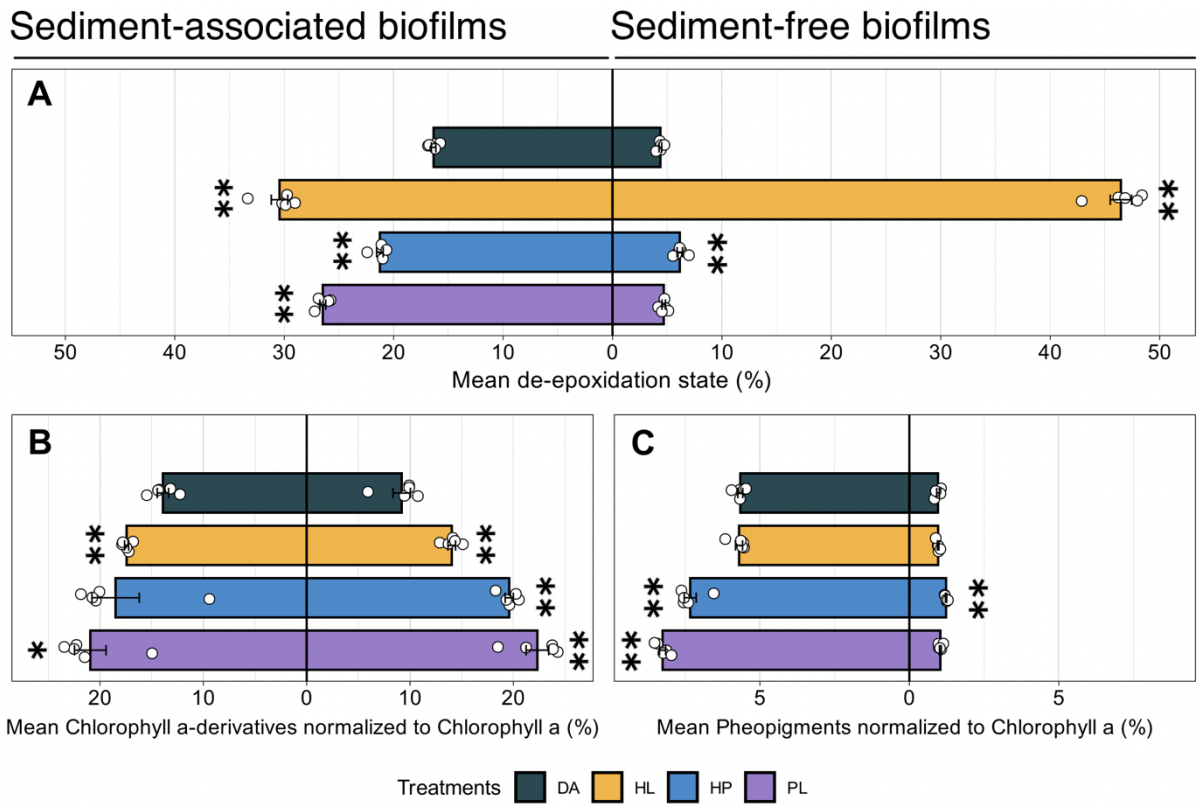

Figure 5. Impact of treatments on pigment content

Barplots showing variations in pigment ratios (%) under the following treatments: Dark-Adapted control (DA), High-Light (HL), Hydrogen Peroxide (HP), and Cold Atmospheric Plasma (PL), for both sediment-associated (left panel) and sediment-free biofilm (right panel) communities; ***A.*** *Barplots of the de-epoxidation state (%);* ***B.*** *Barplots of Chlorophyll a-derivatives pigment ratios;* ***C.*** *Barplots of Pheopigments pigment ratios. Statistical differences were assessed by the Mann-Whitney U test between the dark-adapted control biofilm samples and each stress (n = 5; P < 0.05 *, < 0.01 **).*

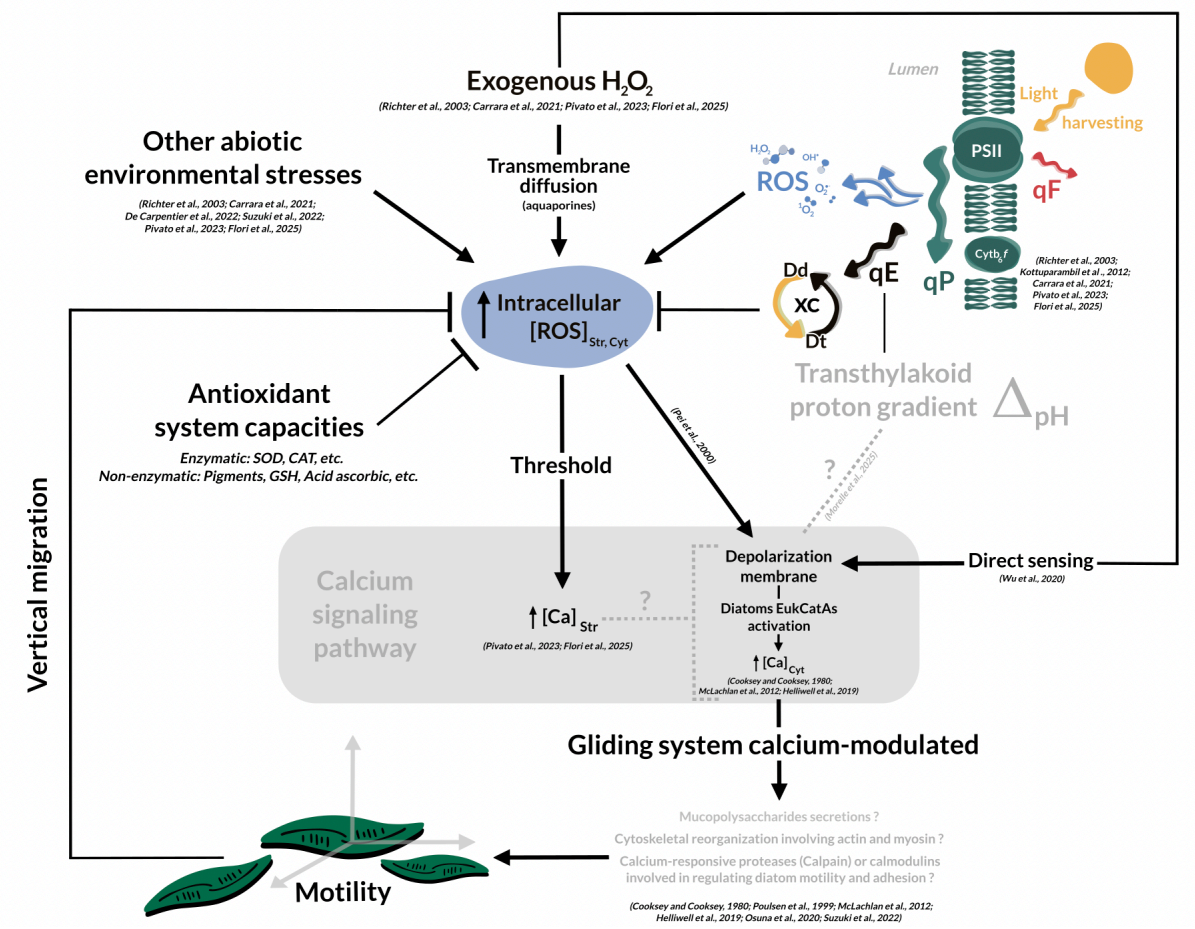

Figure 6. Putative integration of ROS-calcium cellular signaling underlying stress-induced downward vertical migration

Summary of the ROS-Calcium-Motility interplays illustrating a hypothetical signaling model linking the observed motile behavior to the applied stresses. Black arrows and their direction indicate relationships supported by the literature between specific components. Grey dashed lines represent hypothetical interactions. Lines (⊥) indicate processes involved in regulating intracellular ROS concentrations. Abbreviations used in the figure: "qF" fluorescence quenching; "qP" photochemical quenching; "qE" energy-dependent quenching; "str" stromal; "cyt" cytosolic.